Super Low Density InGaAs Semiconductor Ring-Shaped Nanostructures

ARTICLE *in* CRYSTAL GROWTH & DESIGN · JUNE 2008

Impact Factor: 4.89 · DOI: 10.1021/cg701263c

7 AUTHORS, INCLUDING:

Morgan E Ware
University of Arkansas
88 PUBLICATIONS **970** CITATIONS
SEE PROFILE

E. A. Stinaff
Ohio University
47 PUBLICATIONS **979** CITATIONS
SEE PROFILE

Gregory Salamo
University of Arkansas
633 PUBLICATIONS **9,115** CITATIONS
SEE PROFILE

CRYSTAL GROWTH & DESIGN
2008
VOL. 8, NO. 6
1945–1951

Super Low Density InGaAs Semiconductor Ring-Shaped Nanostructures

Jihoon H. Lee,*,† Zhiming M. Wang,† Morgan E. Ware,† Kushal C. Wijesundara,‡ Mauricio Garrido,‡ Eric. A. Stinaff,‡ and Gregory J. Salamo†

Institute of Nanoscale Science and Engineering (INSE), University of Arkansas, Fayetteville, Arkansas 72701, and Department of Physics & Astronomy, Ohio University, Athens, Ohio 45701

Received December 22, 2007; Revised Manuscript Received January 15, 2008

ABSTRACT: We report on the ability to fabricate super low density InGaAs semiconductor ring-shaped nanocrystals on a GaAs (100) surface by molecular beam epitaxy. Specifically, we demonstrate densities down to 2.3×10^6 cm^{-2} with only self-assembled methods based on droplet epitaxy. This is several orders of magnitude lower than conventional nanostructures. The formation of these ring-shaped nanostructures is driven by a self-assembled indium nanodrilling mechanism and diffusion during crystallization.

1. Introduction

During the past decade, enormous research efforts have been dedicated to the growth and fabrication of advanced semiconductor nanostructures including quantum wells,[1] quantum wires,[2] quantum dots (QDs),[3] QD-molecules,[4] and quantum rings (QRs)[5] and other related nanostructures.[6–8] These nanostructures have demonstrated unusual physical, optical, and electrical properties due to their exhibited quantum confinement. These unique and in many cases tunable properties open up a very rich field of device engineering.

Just like QDs, semiconductor QRs have demonstrated atomlike energy levels due to their confinement, which makes them potentially applicable in electronics, optics, and quantum information processing.[9–13] In addition, the Aharonov-Bohm effect[14–16] and unique magnetic susceptibility[17–19] can also be explored with semiconductor QRs. Ring-shaped nanostructures have been fabricated through several approaches including thin layer capping of QDs with a few nm of GaAs,[20–25] postgrowth annealing process,[26,27] Stranski−Krastanow (SK) self-assembled growth[28,29] and droplet epitaxy.[5,30–32] Most of the self-assembled quantum ringlike structures were demonstrated by applying a few nanometers of GaAs on self-assembled InAs QDs.[22–27] Upon the deposition of a thin layer of GaAs, a remarkable morphological change of InAs QDs takes place, thus resulting in quantum ringlike nanostructures. The formation mechanism is understood as being driven by the reduction of the surface free energy of InAs due to the deposition of a thin layer of GaAs.[22–27] Nanoscopic InGaAs ring structures are then fabricated by inserting a short annealing phase after the InAs QDs have been covered by a thin layer of GaAs. While many of the approaches utilize the conversion of QDs to QRs, the following two approaches directly form ring-shaped nanostructures.[28,29] Self-assembled growth of type II GaSb quantum ring structures on GaAs by molecular beam epitaxy was reported to spontaneously form ring-shaped nanostructures as a consequence of the exchange reaction of Sb with As atoms.[28] Most recently, self-assembled formation of concentric quantum double rings with high uniformity and excellent rotational symmetry[5] and the evolution between lattice-matched GaAs/Al0.3Ga0.7As single and double ring-like nanostructures is demonstrated[32] by using the droplet epitaxy technique. In droplet epitaxy, group III elements are applied on the surface under the absence of the supply of group V elements, creating liquid metal droplets. The formation mechanism of group III metal droplets such as Ga, Al, and In is explained by the Volmer–Weber growth mode,[33] in which the bonding energy between incoming group III atoms (adatoms) is much higher than the bonding energy between the surface and the adatoms. Newly formed liquid metal droplets are then converted into semiconductors under the supply of group V flux. Ring-shaped nanostructures were formed though the control of surface diffusion of atoms during the crystallization process.[30–32]

Despite the success of various fabrication approaches of QRs and ring-shaped nanostructures, the density of resulting nanostructures is typically in the range of 10^{10} to 10^{11} cm^{-2} using the conversion of SK grown QDs and between 10^8 and 10^{11} for droplet epitaxial approach. When forming QRs by the conversion of SK grown QDs, the lowest densities that are reasonably achievable are in the range of $\sim 10^9$ cm^{-2}, which is about the lower limit for SK QD formation.[22–28,32] In the droplet epitaxy approach, the density of the resulting nanostructures is in a similar fashion also dependent on the initial density of metal droplets. During the crystallization or converting process, the density of resulting nanostructures stays almost the same as that of metal droplets. Meanwhile, to study the property of QRs, for example, single QR spectroscopy,[5] further processing is still required such as the deposition of submicron metal apertures or the etching of submicron mesas.[5] Other approaches to realize low density QDs have been demonstrated including patterning substrate,[34] making grooves on the substrate,[35] and providing tilt-angle from the flux of atoms.[36] At this point, nevertheless, the fabrication of ring-shaped nanostructures is typically in the range between 10^{10} and 10^{11} cm^{-2} and in some special case it has reached as low as 108 cm^{-2} and thus the growth of lower-density ring-shaped nanostructures is a growth challenge.

In this paper, we report on the formation of InGaAs ring-shaped nanostructures with an extremely low density of $\sim 10^6$ cm^{-2} on GaAs (100) surface by molecular beam epitaxy (MBE). This is several orders of magnitude lower than currently existing growth approaches. We utilized a droplet epitaxy (DE) approach for which the formation mechanism is suggested to be a combination of a nanodrilling process induced by intermixing of In and Ga atoms at the surface and a diffusion process during the crystallization. Figure 1 shows a schematic of the formation process of the InGaAs ring-shaped nanostructures. In this project In metal droplets are formed at several growth temperatures in

* To whom correspondence should be addressed. E-mail: zmwang@uark.edu.
† University of Arkansas.
‡ Ohio University.

10.1021/cg701263c CCC: $40.75
Published on Web 05/20/2008

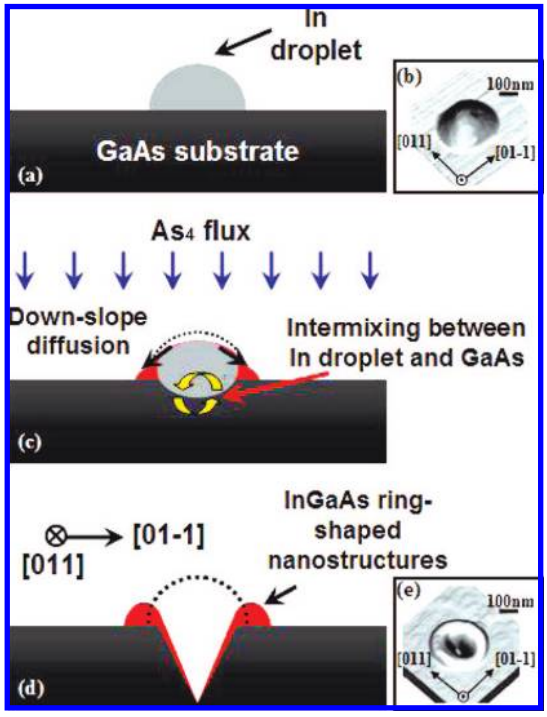

Figure 1. A schematic illustration and three-dimensional (3D) AFM images of the formation of In droplets on GaAs (100) surface in panels (a) and (b). (c) The down-slope diffusion and intermixing process (nanohole drilling) when As_4flux is applied to In droplets. As a result of these combined processes, semiconductor InGaAs ring-shaped nanostructures are formed which are displayed in (e) with a 3D AFM image with its cross-section along [01$\bar{1}$] depicted in (d).

the absence of arsenic atoms on GaAs (100) surface in Figure 1a. The density of ring-shaped nanostructures is predetermined by the density of In droplets, which decreases at higher substrate temperatures. The inset of Figure 1b shows an In metal droplet formed at 350 °C. Subsequently, the In droplets were exposed to incoming As_4 flux for 2 min as shown in Figure 1c. With the applied As_4 flux, the surface energy is redistributed and the droplets go through outward diffusion. Meanwhile during this process, the surface diffusion and rigorous intermixing at the interface between In droplets and GaAs surface and the escape of As atoms from GaAs matrix occur. After this multiphase process, the resulting configuration is the ring-shaped nanostructures in Figure 1d,e. The resulting rings are much shorter and somewhat wider than the original droplets due to the nature of fabrication processes.

2. Experimental Procedures

In this work, nanostructures were grown on a square piece (1.8 × 1.8 cm) of semi-insulating (SI) GaAs substrates by solid-source molecular beam epitaxy (MBE: Riber ^{32}P). Each square substrate was cleaved from 650 μm-thick 3-in. wafers. The cleaved substrate was then mounted on a molybdenum holder held by pins and introduced to a degas chamber. To remove water molecules as well as other contaminants, substrates were degassed at 350 °C for half an hour at ~5×10^{-10} Torr in a separate degas chamber. After a degassing process, the molybdenum holder was moved to the growth chamber. Under highly overpressured As_4 flux (a beam equivalent pressure (BEP) of 5.0 μTorr), the surface oxide was thermally desorbed to grow a defect-free GaAs buffer layer for 10 min. Subsequently, 0.5 μm of GaAs buffer was grown at 600 °C. A 10-min growth interruption was inserted right after buffer layer growth to stabilize the GaAs buffered surface matrix. The nominal growth rate of GaAs was 1.0 monolayer per second (ML/s), which was deduced by in situ reflection high energy electron diffraction (RHEED). After the GaAs buffer growth, a (2 × 4) surface

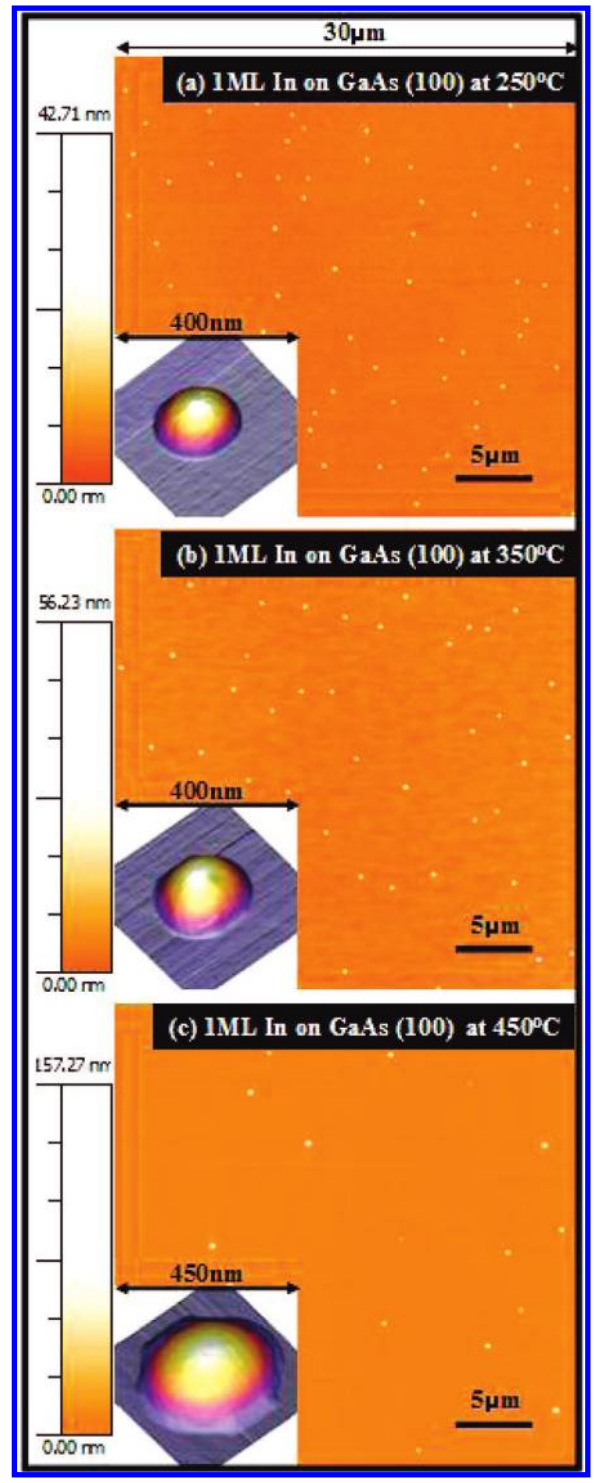

Figure 2. The formation In droplets with 1 monolayer (equivalent amount of InAs) deposition on GaAs (100) surface for each growth temperatures: (a) at 250 °C, (b) at 350 °C, (c) at 450 °C. The large scale two-dimensional (2D) AFM images are 30 × 30 μm areas and the color scale bars located on the left sides are applied for vertical scale respectively. Insets are 3D AFM images are 450 × 450 nm and show a representing size and shape of In droplets at each growth temperature.

reconstruction was observed at 600 °C. For the formation of the In droplets in Figure 2, the substrate was then reduced to each of the growth temperatures: 250, 350, and 450 °C. During the reduction of surface temperature, the surface was initially exposed to a BEP of 5.0 μTorr of highly overpressured As_4 flux which was then turned off at ~500 °C. Throughout this range the surface went through various

reconstructions. For example, while heading to the target surface temperature, at ~540 °C, the surface reconstructed to C(4 × 4) and became (2 × 4) again when the As_4 flux was eliminated at ~500 °C. Also, after deposition of In, the (2 × 4) surface was reconstructed to (4 × 2). After reaching the growth temperature, the growth was paused until the background pressure of below 3×10^{-9}Torr was reached in the chamber in order to minimize the effect of background arsenic pressure as much as possible. 1 ML (an equivalent amount of InAs when As is supplied) of In was applied at 250, 350, and 450 °C, which formed the droplets. Subsequently, the In droplets were exposed to an As_4 flux at each growth temperature. In droplet epitaxy, the exposing of metal droplets to incoming group V element is known as crystallization and/or arsenization.[37] This process converts the liquid metal group III droplets into crystals such as GaAs, AlAs, and InAs. Two different As_4 fluxes were applied for the crystallization of In droplets into InGaAs ringlike nanostructures. For the results in Figures 3 and 4, the As valve was 100% open and this generated a BEP of 5.0 μTorr of As_4 flux. For the results in Figure 5a, a BEP of 0.5 μTorr of As_4 flux was applied from the valve-controlled solid source As cell. Maintaining constant As flux, the samples were quenched immediately following the termination of each growth. An atomic force microscope (AFM: Veeco 3100) in air was used to see the morphology of nanostructures. Finally, identical samples grown at 350 and 450 °C were capped with 70 nm of GaAs at 500 °C for optical measurements. Photoluminescence was performed in a pseudoconfocal configuration in a closed cycle cryostat at 20 K, which allowed for the identification of features from individual nanostructures due to their low density.

3. Results and Discussion

In droplet epitaxy, the initial dimension of the droplets and the diffusion process determine the size and shape of the resulting nanostructures. In addition, the density of nanostructures is also typically predetermined by the initial density of liquid metal droplets. Therefore, it is important to take a close look at the dimensions and the density of initial droplets. Figure 2 shows the formation of In droplets at each surface temperature on GaAs (100) surfaces: (a) 1 ML In at 250 °C, (b) 1 ML In at 350 °C and (c) 1 ML In at 450 °C. The large scale pictures are two-dimensional (2D) atomic force microscopy (AFM) images of 30 × 30 μm area and the insets are three-dimensional (3D) AFM images of 400 × 400 nm. The vertical color-scale bar given on the left side of each image is related to the large figures. In general, In droplets are circular in shape and this can be because the equilibrium configuration; that is, the liquid In droplets prefers the minimum surface area based on the Volmer-Webber growth model.[33] The average density of In droplets was 7.4×10^6 cm^{-2} at 250 °C, 5.0×10^6 cm^{-2} at 350 °C, and 2.3×10^6 cm^{-2} at 450 °C, which means just a few to several droplets per each 10 μm^2. This is very promising for the realization of ultra low-density quantum and nanostructure fabrication. In general the In droplets form with a lower density at higher substrate temperatures, which was reported in our previous work on the critical thickness for In droplet formation[38] and also observed in Ga metal droplets.[39] The average dimensions of In droplets were respectively for the 250, 350, and 450 °C samples: 45, 60, and 130 nm for the height and 200, 250, and 380 nm for the diameter at the base of the droplets. Therefore, while the density decreases with increasing temperature, the average dimensions of each of the droplets increase. This seems consistent with a ripening process which is thermally activated. It is interesting to note, here, that the increase in dimensions is exponential proportionately larger going from 350 to 450 °C than it is in going from 250 to 350 °C. This is also consistent with a thermally activated process.

The next step to fabricate semiconductor quantum- and nanostructures by droplet epitaxy is to expose these liquid metal droplets to a group-V flux in order to form crystalline materials converting liquid droplets into semiconductors. This is typically

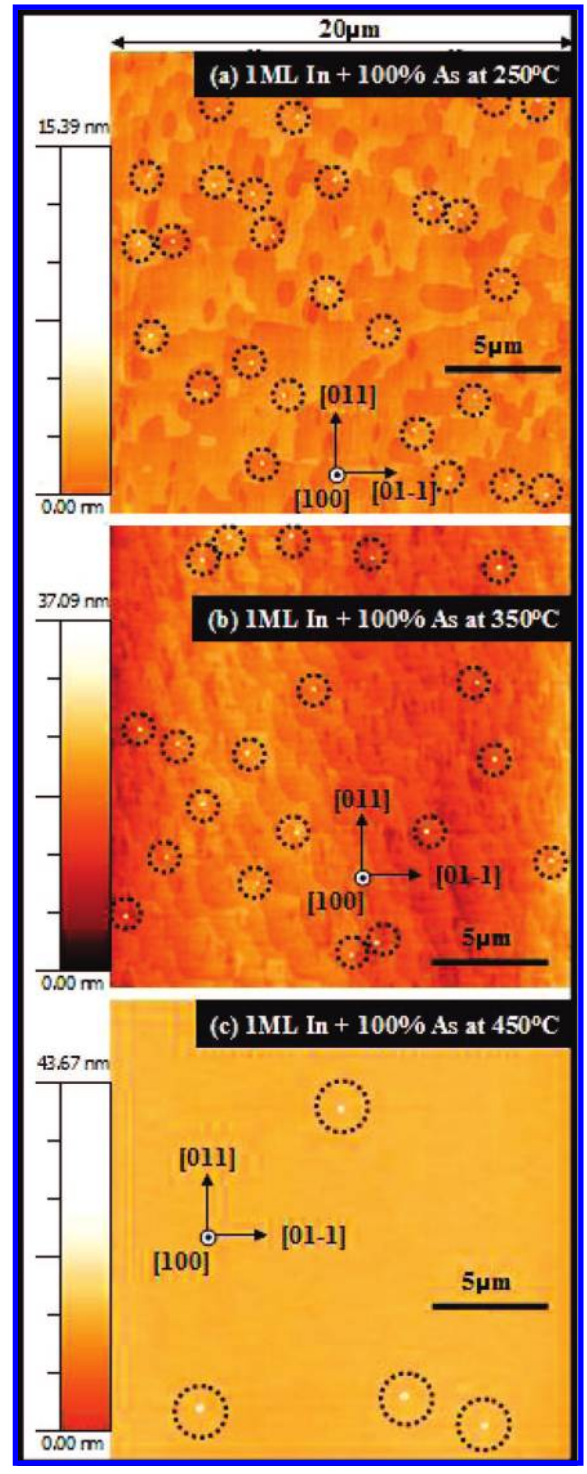

Figure 3. As a result of the exposure of In droplets to subsequent As flux, ring-shaped nanostructures were formed: (a) at 250 °C, (b) at 350 °C, (c) at 450 °C. The dotted circles show the positions of the nanostructures in each frame. The 2D AFM images are 30 × 30 μm areas and the color scale bars are applied for vertical scale for each picture.

known as arsenization due to the nature of this process.[32,37] This general technique has been demonstrated well in arsenide-based semiconductors converting Ga, Al, and In metal droplets into GaAs, AlAs, and InAs.[30–32,37] Figure 3 shows 20 × 20 μm AFM images of the crystallized structures. The In droplets were exposed to As atoms for 2 min right after the droplet formation without varying the temperature. Dotted circles indicate the

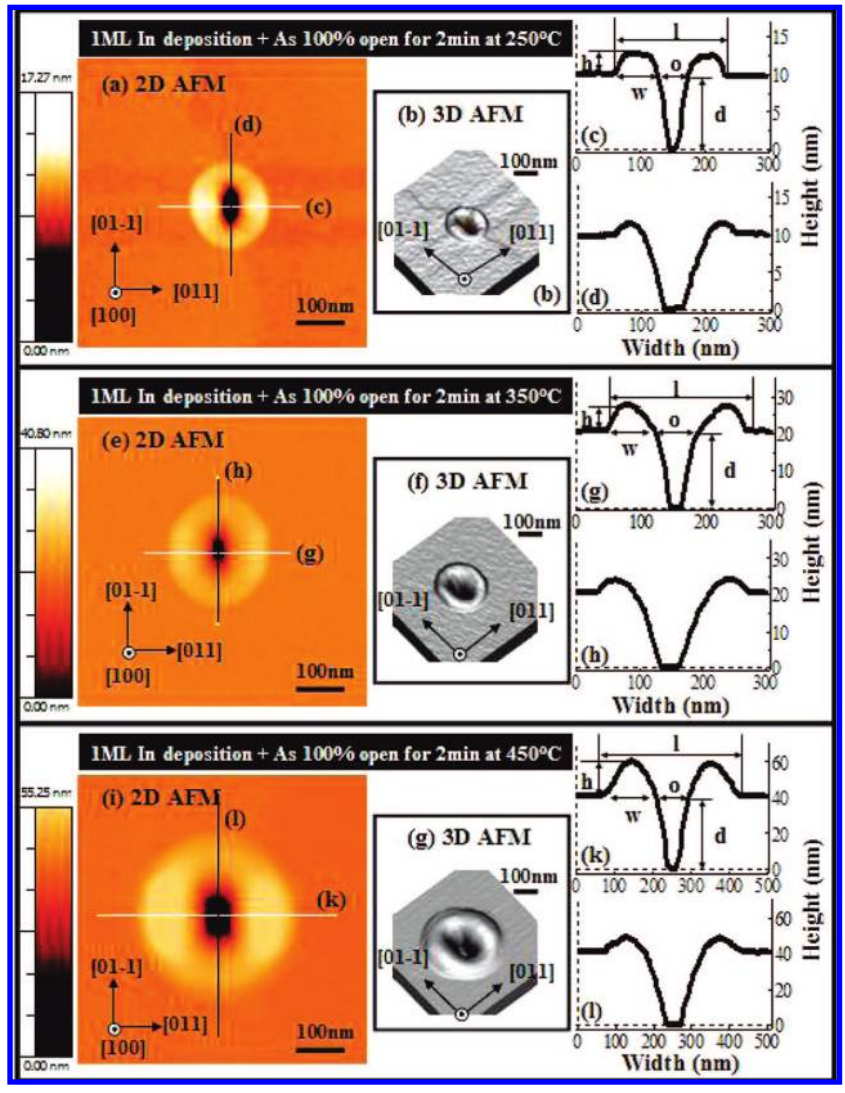

Figure 4. Individual semiconductor ring-shaped nanostructures formed at different growth temperatures are presented with 2D top-view, 3D tilted-view AFM images and cross-sectional line-profiles along two noteworthy directions. These enlarged images from the same are of the samples as Figure 3 provide detailed views of each structure. Both 2D and 3D AFM images are 600 × 600 nm areas and the cuts for the line-profiles are shown in the 2D AFM images.

location where the ring-shaped nanostructures were formed. The corresponding average density of resulting nanostructures was respectively 7.7×10^6 cm^{-2}, 4.7×10^6 cm^{-2}, and 1.5×10^6 cm^{-2} at 250, 350, and 450 °C. This is in quite good agreement with the initial density of droplets at each temperature. With this result, we conclude that virtually all of the droplets were converted into nanostructures rather than diffusing away during the crystallization process, as has been observed for the arsenization of Ga droplets into GaAs quantum ringlike nanostructures.[30–32,37]

Figure 4 presents a close picture of the InGaAs rings formed at each temperature. 3D projections of the 600 × 600 nm, 2D AFM images on the left are shown in the middle. The right column in Figure 4 shows cross-sectional line-profiles from the images on the left in the directions given. In each line-profile, the height, width, outer-diamter, width of hole (inner diameter), and depth of hole are given by *h*, *w*, *l*, *o*, and *d*, respectively. The applied As_4 flux for this set was fixed at a BEP of 5.0 μTorr for all three samples, which was 100% valve-open position. The detailed dimensions of resulting ring-shaped nanostructures are given in Table 1.

Here we propose a combined growth mechanism of InGaAs ring-shaped nanostructures. Indeed, the resulting structure is most likely composed of InGaAs due to interfacial intermixing induced by the nanodrilling of the droplets. Nanodrilling indicates an exchange and/or merging process of atoms at the interface between In droplets and GaAs surface as indicated in Figure 1. At the interface, there is a severe intermixing and/or exchanging of Ga and In atoms. At the same time, As atoms associated with the Ga can easily be sucked into In droplets in order to equilibrate the energy between GaAs matrix and In droplets. This can be because In droplets are highly unstable in the presence of As atoms and try to form crystalline InAs. Even for the growth of traditional S−K InAs quantum dots, whose system should be much more stable than In droplets, a severe intermixing of In and Ga atoms on the GaAs surface was observed when a long additional annealing time was given and finally all the In atoms merged into GaAs matrix after 10 min and InAs quantum dots completely disappeared.[40] Once As atoms incorporate into the In matrix, according to the phase diagram of InAs, As atoms cannot exist within the In matrix. Therefore, the As atoms keep traveling out of the droplets and

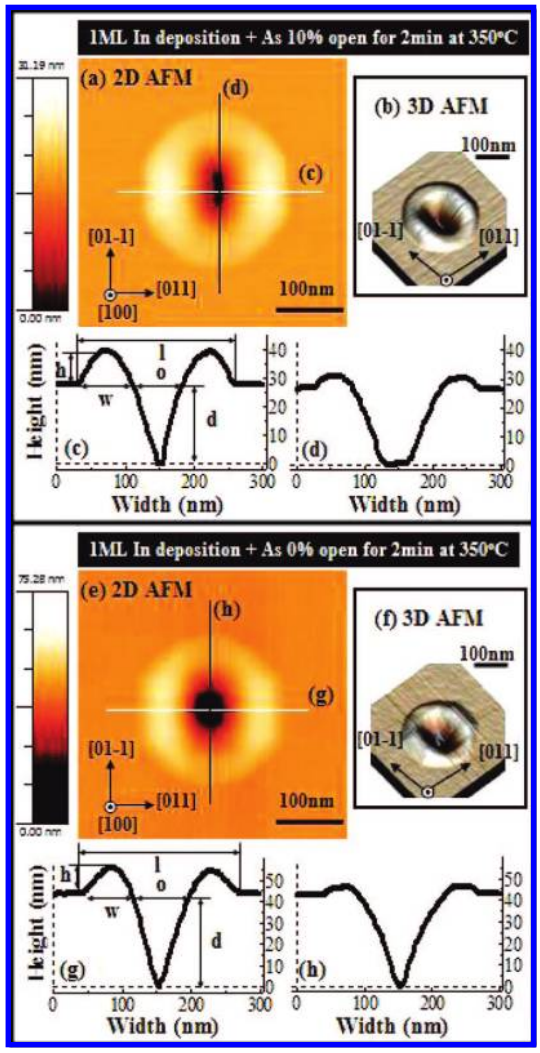

Figure 5. The formation of semiconductor ring-shaped nanostructures with different As pressures supplied at 350 °C to see the effect of changing As pressure for a fixed substrate temperature. The 2D and 3D AFM images are 400 × 400 nm areas and again the cuts for the line-profiles are shown in the 2D AFM images.

Table 1. Average Dimensions of Ring-Shaped Nanostructures

T (°C) & As[a]	*D* & No.[b]	*h* (nm)[c]	*W* (nm)[d]	*o* (nm)[e]	*l* (nm)[f]	*d* (nm)[g]
250/100%	[011] 4(c)	3	60	50	180	10
	[01$\bar{1}$] 4(d)	2	50	100	200	
350/100%	[011] 4(g)	7	70	80	220	21
	[01$\bar{1}$] 4(h)	3	60	130	250	
450/100%	[011] 4(k)	19	120	90	330	41
	[01$\bar{1}$] 4(l)	9	100	160	360	
350/10%	[011] 5(c)	13	80	70	230	27
	[01$\bar{1}$] 5(d)	5	60	130	250	
350/0%	[011] 5(g)	8	75	85	235	43
	[01$\bar{1}$] 5(h)	4	55	125	250	

[a] Sample growth temperature/the percentage of As valve open position, that is, 100% and 10% valve open. [b] Direction of line-profile and associated figure number. [c] Height of ring from the surface but not from the bottom line (zero) in vertical scale. [d] Width of ring at the surface. [e] Width of nanohole opening. [f] Diameter of ring. [g] Depth of nanohole.

finally either escape out of the droplets or form InAs on the edge of droplets, at the base near the substrate. Thus, In droplets keep merging with underlying GaAs matrix and, as a result, form nanoholes right underneath the droplets. At the same time, the In droplets are exposed to an incoming flux of As atoms, which is known to encourage the downward-slope diffusion of atoms from the top of the droplets,[41] thus forming InAs around the bottom edge of the droplets. Again, the As atoms cannot exist within the In matrix and thus the In atoms would keep diffusing downward and form InAs around droplets. In short, there are two mainstream growth mechanisms that drive the formation of these interesting ring-shaped nanostructures: nanodrilling and diffusion. The formation of the nanoholed ring-shaped nanostructures is the direct result of the combination of both.

Now let us take a close look at what these ring-shaped nanostructures look like and how differently they formed at each different growth temperature. First of all, the ring-shaped nanostructures are not perfectly circular but in fact the lateral length, *l*, of the nanostructures is somewhat larger along the [01$\bar{1}$] direction by ∼10% at 250 °C, ∼14% at 350 °C, and ∼9% at 450 °C: overall, about 10% wider along the [01$\bar{1}$] direction. This can be due to the highly anisotropic nature of the diffusion process on GaAs surface. The (2 × 4) reconstructed GaAs (100) surface possesses a highly anisotropic surface diffusion between the [01$\bar{1}$] and [011] directions due to the atomic corrugation induced by the reconstructed dimer rows. This corrugation is much higher along the [01$\bar{1}$] direction.[42] In addition, the rings are taller (h) and wider (w) along the [011] direction as compared to the [01$\bar{1}$] direction: taller and wider by ∼50% and ∼20% at 250 °C, ∼130% and ∼16% at 350 °C and ∼110% and ∼20% at 450 °C. We do not know quantitatively how anisotropic the diffusion is on this surface, especially with In droplets formed; however, this still seems like a valid explanation for the elongation found in our structures as there seems to be a lot of material diffused away along [01$\bar{1}$] resulting in shallower and narrower rings. As a result, the openings of the nanoholes are also not perfectly circular as clearly seen in the 2D top-views in Figure 4a,e,i. The openings are wider in the direction of higher diffusion, that is, along the [01$\bar{1}$] direction. From this result, we can presume the initial stage of ring-shaped nanostructure formation. That is, initially a great amount of In begins diffusing along the [01$\bar{1}$] direction with the supplied As flux and, at the same time, underneath of the droplets As atoms are drawn into the In droplets. Therefore, In atoms intermix with Ga atoms, and As atoms keep traveling out of the In matrix. This creates the nanoholes underneath the In droplets. The depth of hole (*d*) of the ring-shaped nanostructures increases with the growth temperature. It is 10 nm, 21 nm, and 41 nm at 250, 350, and 450 °C, respectively, as shown in Table 1. With every 100 °C increase, the depth of nanoholes is increased by almost a factor of 2. This behavior can be strongly related to two factors: the surface temperature and the size of droplets. As discussed above, the droplet size is larger with higher growth temperature due to the higher diffusion of surface adatoms. With more material in the droplet, nanodrilling can last longer creating a deeper hole, because the merging and exchanging of atoms will keep progressing until all the In has been crystallized.

Figure 5 shows 2D top-view and 3D side-view AFM images and line-profiles along [011] and [01$\bar{1}$] of InGaAs ringlike nanostructures crystallized at 350 °C with 1 ML deposition. In distinction from results in Figures 3 and 4, two different As_4 fluxes were used for this set. Figure 5a shows the result of crystallization with the As valve at 10% supplying a BEP of 0.5 μTorr, and Figure 5e shows the result of crystallization with the As valve closed having only background As. Detailed measurements of the dimensions of the resulting structures are given in Table 1. The results of crystallization with the As valve

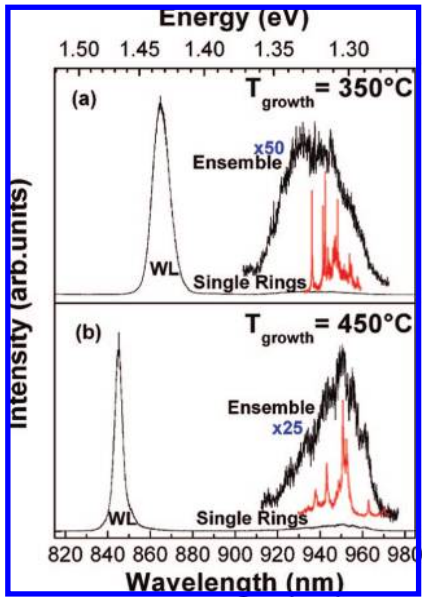

Figure 6. Photoluminescence taken at 20 K from ring-shaped nanostructure samples formed at (a) 350 °C and (b) 450 °C. Ensemble spectra in each case is shown magnified with respect to the wetting layer (WL) of the same spectra and taken using 750 nm laser excitation with a power density of ~1–10 W/cm^2. Single ring spectra were taken in a pseudoconfocal configuration as allowed for by the low density of rings using 780 nm laser excitation with a power density of ~0.001–0.01 W/cm^2. The large number of narrow lines in the single ring spectra is thought to be due to the high energy excitation and the arbitrary power density causing multiexciton and multicharged recombinations.

10% open are quite similar in terms of dimensions of resulting ring-shaped nanostructure as compared to the 100% open samples. In both cases, the heights of the rings (h) are more than twice taller along the [011] directions, and widths of rings (w) are somewhat wider along [011]. Meanwhile, the widths of nanohole openings are much wider along [01$\bar{1}$] and the diameters of the rings are larger along the [01$\bar{1}$] direction. As discussed, these results can be again due to the anisotropic nature of this GaAs surface. Although the dimensions are not exactly the same for the sample crystallized with the As valve closed, the general tendency is the same for all the dimensions. There is one distinctive difference, though, and that is the depth of nanoholes (d). With As valve 100% open, the value of d is 21 nm, with 10% open, it is 27 nm and it is 43 nm with 0% As open. The depth of hole is almost twice as deep when the droplets are crystallized with no As flux supplied. This can be due to the delayed crystallization of In droplets. With much less As atoms supplied, the combining process of In and As atoms was further delayed and this provided much more In atoms that can contributed to the nanodrilling process. This is interesting since the depth of nanoholes can be controlled by controlling the As pressure. This tuneability was not evident from studies[32] of the crystallization of Ga droplets where it was found that double ring-shaped nanostructures were formed with As 100% open and single ringlike nanostructures were the results of As 10% open.

Finally, as a measure of the quantum confined nature of these ringed structures, samples were grown with rings formed at 350 and 450 °C followed by a capping layer of 70 nm GaAs. These samples were used for photoluminescence (PL) measurements, Figure 6. Most notably, for both samples, when the excitation power is reduced sufficiently, ~mW/cm^2, and a small enough region of the sample is examined, the PL breaks up into many narrow lines as was seen in the very early single QD PL measurements[43] but only after etching sub-micrometer mesas in the samples by laborious electron beam lithography. This strongly indicates that we are looking at a system with 3D confinement like QDs, exhibiting discrete and narrow PL transitions. A sample region small enough was easily isolated by a pseudoconfocal approach, which consisted of focusing the light from the sample, collected by a long working distance microscope objective, onto the narrow entrance slit of a spectrometer, ~10 μm, and collecting data from only a small region of the CCD camera attached to the spectrometer, ~100 μm, in the nondispersive direction. We estimate this to give us a field of view on the sample of on the order of ~1–10 μm.

In comparing the two samples of Figure 6 we find two notable features: first, that there exists a 2D, wetting layer-like (WL) PL peak[44] which shifts between the samples, and, second, that the ensemble PL from the ring structures is at about the same energy for both samples. We see that the WL peak from the sample grown at a higher temperature, 450 °C, is at a higher energy than the WL peak from the 350 °C sample. This is most likely due to increased alloying of the Ga from the substrate during crystallization, but could also be caused by the WL being thinner. At higher temperatures, it would be expected that slightly less In accumulates on the surface during the droplet formation. A combination of both of these effects is probable. Finding that the ring emission is at nearly the same energy for both samples is surprising, because the AFM images of these samples, Figure 4, shows such a dramatic difference in the size of the rings. There is a slight shift to lower energy for the 450 °C sample, but it is not enough to account for the size difference. This may indicate that there is some equilibrium size or shape that the rings form after capping, or that the emission that we observe is from some substructure of the ring, the dimensions of which are not varied in the experiment.

4. Conclusions

Droplet epitaxy was used to fabricate super low density semiconductor ring-shaped InGaAs/GaAs nanostructures on GaAs (100) surface by MBE. The effects of changing the substrate temperature and As flux during droplet formation and crystallization were investigated. The resulting density of nanostructures could be as low as in the range of ~10^6 cm^{-2} for all investigated substrate temperatures, which is only a few nanostructures per each 10 μm^2. It was also determined that the density of converted nanostructures was strictly governed by the initial density of droplets. The roles of nanodrilling and surface diffusion were discussed for the mechanisms responsible for the formation of these ring-shaped nanostructures. The control of the diameter, width, and height of nanostructures as well as the depth of the hole was demonstrated by controlling the growth environment. And, finally, PL measurements were performed which demonstrated the high crystalline quality of these nanostructures, and that they do exhibit confinement. This result is a unique approach to fabricate unusually low density of ring-shaped semiconductor nanostructures and also an easy and flexible growth approach to study properties of these nanostructures without further processing.

Acknowledgment. The authors acknowledge the financial support of the NSF (through Grant DMR-0520550).

References

(1) Miller, D. A.; Chemla, D. S.; Damen, T. C.; Gossard, A. C.; Wiegmann, W.; Wood, T. H.; Burrus, C. A. *Phys. Rev. B* **1985**, *32*, 1043.

(2) Wegscheider, W.; Pfeiffer, L. N.; Dignam, M. M.; Pinczuk, A.; West, K. W.; McCall, S. L.; Hull, R. *Phys. Rev. Lett.* **1993**, *71*, 4071.
(3) (a) Stinaff, E. A.; Scheibner, M.; Bracker, A. S.; Ponomarev, I. V.; Korenev, V. L.; Ware, M. E.; Doty, M. F.; Reinecke, T. L.; Gammon, D. *Science* **2006**, *311*, 636. (b) Lingmin Kong; Wu, Z.; Feng, Z. C.; Fergusonan, I. T. *J. Appl. Phys.* **2007**, *101*, 126101.
(4) (a) Lee, J. H.; Wang, Z. M.; Strom, N. W.; Mazur Yu, I.; Salamo, G. J. *Appl. Phys. Lett.* **2006**, *89*, 202101. (b) Suraprapapich., S.; Panyakeow, S.; Tu, C. W. *Appl. Phys. Lett.* **2007**, *90*, 183112. (c) Li, S.-S.; Xia, J.-B. *Appl. Phys. Lett.* **2007**, *91*, 092119. (d) Beirne, G. J.; Hermannstä dter, C.; Wang, L.; Rastelli, A.; Schmidt, O. G.; Michler, P. *Phys. Rev. Lett.* **2006**, *96*, 137401.
(5) Mano, T.; Kuroda, T.; Sanguinetti, S.; Ochiai, T.; Tateno, T.; Kim, J.; Noda, T.; Kawabe, M.; Sakoda, K.; Kido, G.; Koguchi, N. *Nano Lett.* **2005**, *5*, 425.
(6) (a) Liang, B. L.; Wang, Zh. M.; Lee, J. H.; Sablon, K.; Mazur, Yu. I.; Salamo, G. J. *Appl. Phys. Lett.* **2006**, *89*, 043113. (b) Alonso-González, P.; Alén, B.; Fuster, D.; González, Y.; Gonzále, L.; Martínez-Pastor, J. *Appl. Phys. Lett.* **2007**, *91*, 163104.
(7) (a) Wang, X.; Wang, Z. M.; Liang, B.; Salamo, G. J.; Shih, C.-K. *Nano Lett.* **2006**, *6*, 1847. (b) Alonso-González, P.; González, L.; González, Y.; Fuster, D.; Fernández-Martı´nez, I.; Martı´n-Sánchez, J.; Abelmann, L. *Nanotechnology* **2007**, *18*, 355302.
(8) (a) Wang, Z. M.; Liang, B.; Sablon, K. A.; Lee, J.; Mazur Yu, I.; Strom, N. W.; Salamo, G. J. *Small* **2007**, *3*, 235. (b) Kanto, T.; Yamaguchi, K. *Jpn. J. Appl. Phys.* **2005**, *44*, 7690.
(9) Warburton, R. J.; Schäflein, C.; Haft, D.; Bickel, F.; Lorke, A.; Karral, K.; Garcia, J. M.; Schoenfeld, W.; Petroff, P. M. *Nature* **2000**, *405*, 926.
(10) Fuhrer, A.; Lüscher, S.; Ihn, T.; Heinzel, T.; Ensslin, K.; Wegscheider, W.; Bichler, M. *Nature* **2001**, *413*, 822.
(11) Ivanov, M. V.; Schmelcher, P. *J. Phys.: Condens. Matter* **2006**, *18*, 2963.
(12) Li, S.-S.; Xia, J.-B. *J. Appl. Phys.* **2001**, *89*, 3434.
(13) Lorke, A.; Luyken, R. J.; Govorov, A. O.; Kottaus, J. P. *Phys. Rev. Lett.* **2000**, *84*, 2223.
(14) (a) Bayer, M.; Korkusinski, M.; Hawrylak, P.; Gutbrod, T.; Michel, M.; Forchel, A. *Phys. Rev. Lett.* **2003**, *90*, 186801. (b) Kleemans, N. A. J. M.; Bominaar-Silkens, I. M. A.; Fomin, V. M.; Gladilin; Granados, D.; Taboada, A. G.; Garcı´a, J. M.; Offermans, P.; Zeitler, U.; Christianen, P. C. M.; Maan, J. C.; Devreese, J. T.; Koenraad, P. M. *Phys. Rev. Lett.* **2007**, *99*, 146808.
(15) Gefen, Yu.; Imry, Y.; Azbel, M. Ya. *Phys. Rev. Lett.* **1984**, *52*, 129.
(16) Chandrasekhar, V.; Rooks, M. J.; Wind, S.; Prober, D. E. *Phys. Rev. Lett.* **1985**, *55*, 1610.
(17) Chakraborty, T.; Pietiläinen, P. *Phys. Rev. B* **1994**, *50*, 8460.
(18) Climente, J. I.; Planelles, J. *Phys. Rev. B* **2003**, *68*, 075307.
(19) Römer, R. A.; Raikh, M. E. *Phys. Rev. B* **2000**, *62*, 7045.
(20) Offermans, P.; Koenraad, P. M.; Wolter, J. H.; Granados, D.; García, J. M.; Fomin, V. M.; Gladilin, V. N.; Devreese, J. T. *Appl. Phys. Lett.* **2005**, *87*, 131902.
(21) Granados, D.; Garcia, J. M. *J. Cryst. Growth* **2003**, *251*, 213.
(22) Granados, D.; Garcýa, J. M. *Appl. Phys. Lett.* **2003**, *82*, 2401.
(23) Kiravittaya, S.; Songmuang, R.; Jin-Phillipp, N. Y.; Panyakeow, S.; Schmidt, O. G. *J. Cryst. Growth* **2003**, *251*, 258.
(24) Schmidt, O. G.; Deneke, Ch.; Kiravittaya, S.; Songmuang, R.; Heidemeyer, H.; Nakamura, Y.; Zapf-Gottwick, R.; Müller, C.; Jin-Phillipp, N. Y. *IEEE J. Selected Topics in Quantum Electron.* **2002**, *8*, 1025.
(25) Songmuang, R.; Kiravittaya, S.; Schmidt, O. G. *J. Cryst. Growth* **2003**, *249*, 416.
(26) Garc, J. M.; Medeiros-Ribeiro, G.; Schmidt, K.; Ngo, T.; Feng, J. L.; Lorke, A.; Kotthaus, J.; Petroff, P. M. *Appl. Phys. Lett.* **1997**, *71*, 2014.
(27) Lorke, A.; Luyken, R. J.; Garcia, J. M.; Petroff, P. M. *Jpn. J. Appl. Phys. Part 1* **2001**, *40*, 1857.
(28) Kobayashi, S.; Jiang, C.; Kawazu, T.; Sakaki, H. *Jpn. J. Appl. Phys.* **2004**, *43*, L662.
(29) Yu, L. W. ; Chen, K. J.; Song, J.; Xu, J.; Li, W.; Li, H. M.; Wang, M.; Li, X. F.; Huang, X. F. *Adv. Mater.* **2007**, *19*, 1577.
(30) Huang, S.; Niu, Z.; Fang, Z.; Ni, H.; Gong, Z.; Xia, J. *Appl. Phys. Lett.* **2006**, *89*, 031921.
(31) (a) Koguchi, N.; Takahashi, S.; Chikyow, T. *J. Cryst. Growth* **1991**, *111*, 688. (b) Watanabe, K.; Koguchi, N.; Gotoh, Y. *Jpn. J. Appl. Phys. Part 1* **2000**, *39*, L79. (c) Mano, T.; Koguchi, N. *J. Cryst. Grow.* **2005**, *278*, 108.
(32) Lee, J. H.; Wang, Zh. M.; AbuWaar, Z. Y.; Strom, N. W.; Salamo, G. J. *Nanotechnology* **2006**, *17*, 3973.
(33) Volmer, M.; Weber, A. *Z. Phys. Chem.* **1926**, *119*, 277.
(34) Ishikawa, T.; Nishimura, T.; Kohmoto, S.; Asakawa, K. *Appl. Phys. Lett.* **2000**, *76*, 167.
(35) Jin, Peng.; Ye, X. L.; Wang, Z. G. *Nanotechnology* **2005**, *16*, 2775.
(36) Evgenii S., Moskalenko.; Karlsson, Fredrik K.; Donchev, Vesselin T.; Holtz, Per Olof.; Monemar, Bo.; Schoenfeld, Winston V.; Petroff, Pierre M. *Nano Lett.* **2005**, *5*, 2117.
(37) Wang, Z. M.; Kyland, H.; Shultz, J. L.; Salamo, G. J. *Phys. Status Solidi* **2005**, *202*, R85.
(38) Lee, J. H.; Wang, Z. M.; Salamo, G. J. *J. Phys.: Condens. Matter.* **2007**, *19*, 176223.
(39) AbuWaar, Z. Y.; Wang, Z. M.; Lee, J. H.; Salamo, G. J. *Nanotechnology* **2006**, *17*, 4037.
(40) Krzyzewski, T. J.; Jones, T. S. *Appl. Phys. Lett.* **2004**, *96*, 668.
(41) Wang, Z. M.; Liang, B. L.; Sablon, K. A.; Salamo, G. J. *Appl. Phys. Lett.* **2007**, *90*, 113120.
(42) Laukkanen, P.; Kuzmin, M.; Perälä, R. E.; Ahola, M.; Mattila, S.; Väyrynen, I. J. *Phys. Rev. B* **2005**, *72*, 045321.
(43) Marzin, J.-Y.; Gérard, J.-M.; Izraël, A.; Barrier, D.; Bastard, G. *Phys. Rev. Lett.* **1994**, *73*, 716.
(44) Yoffe, A. D. *Adv. Phys.* **2001**, *50*, 1.

CG701263C